

An inverse model for a free-boundary problem with a contact line: Steady case

Oleg Volkov, Bartosz Protas*

Department of Mathematics and Statistics, McMaster University, 1280 Main Street West, Hamilton, Ontario, Canada L8S 4K1

ARTICLE INFO

Article history:

Received 24 March 2008

Received in revised form 4 November 2008

Accepted 31 March 2009

Available online 11 April 2009

PACS:

44.05.+e

64.70.D-

02.30.Zz

Keywords:

Free-boundary problem

Stefan conditions

Contact line

Shape calculus

Sobolev gradients

ABSTRACT

This paper reformulates the two-phase solidification problem (i.e., the Stefan problem) as an inverse problem in which a cost functional is minimized with respect to the position of the interface and subject to PDE constraints. An advantage of this formulation is that it allows for a thermodynamically consistent treatment of the interface conditions in the presence of a contact point involving a third phase. It is argued that such an approach in fact represents a closure model for the original system and some of its key properties are investigated. We describe an efficient iterative solution method for the Stefan problem formulated in this way which uses shape differentiation and adjoint equations to determine the gradient of the cost functional. Performance of the proposed approach is illustrated with sample computations concerning 2D steady solidification phenomena.

© 2009 Elsevier Inc. All rights reserved.

1. Introduction

In this investigation we propose a computational method for solution of heat transfer problems with change of phase, the so-called two-phase Stefan problem, when contact lines are present. Such problems arise in many applications, including the modeling and control of crystal growth [1,2], melting and solidification [3,4], or optimization of advanced welding processes which is the particular problem motivating the present research effort. By a contact line we mean an intersection of the interface separating the two phases (i.e., for example, the liquid and the solid phase) with another interface separating the third phase (i.e., gas), or the domain boundaries. From the mathematical modeling perspective, the main challenge is to derive interface conditions consistent from the physical (thermodynamic) point of view and at the same time computationally tractable. The triple-phase contact problem is a subject of intensive research, both theoretical and experimental. Although significant results have been achieved in both understanding and modeling such problems, it remains unclear whether they can be applied to the case of the molten contact line, see [3,4] for more discussion. Whether or not a contact line is present, the Stefan problem represents a *free-boundary* problem, i.e., one in which the position of the liquid–solid interface is also an unknown and must be determined in addition to solution of the governing partial differential equations (PDEs). We propose here to formulate this problem as an inverse problem which can then be solved using methods of

* Corresponding author. Fax: +1 905 522 0935.

E-mail address: bprotas@mcmaster.ca (B. Protas).

PDE-constrained optimization. In this approach a suitably parametrized geometry of the interface serves as a control variable that is adjusted to satisfy the interface boundary conditions in a suitable sense. The idea of recasting a free-boundary problem as an optimization problem is not new [5], and was already applied in a general setting in the theoretical investigations of Alt and Caffarelli [6], Zolésio [7] and Hoffmann and Tiba [8], while in the context of a one-dimensional (1D) Stefan problem such an approach was considered by Okhezin [9]. From the computational point of view the main difficulty consists in determining the gradient (i.e., the sensitivity) of the cost functional with respect to modifications of the domain geometry, the so-called “shape gradient” [10]. As regards computational studies, applications of this approach to some model problems were explored by Männikkö et al. [11], Tiihonen [12], Kärkkäinen and Tiihonen [13], Haslinger et al. [14], Donaldson and Wetton [15] and Eppler et al. [16,17].

Our present work tackles a more complicated version of the Stefan problem which involves a contact line and a third phase. One contribution of this investigation is to show how the constraints due to the third phase can be incorporated into a consistent formulation of the optimization problem, more specifically, the definition of the shape gradient. Another contribution is to propose and justify a definition of the cost functional that is thermodynamically more consistent than the ones used in previous investigations (e.g. [9,11,14]). It is also shown that the proposed formulation is in fact equivalent to introducing a closure model for the capillary phenomena at the contact line. The structure of the paper is as follows: in the next Section we present the mathematical framework for the Stefan problem with a particular focus on the interface boundary conditions, in the following Section we reformulate this problem as an optimization problem, whereas an adjoint-based algorithm for its solution is introduced in Section 4; computational results are presented and discussed in Section 5; summary and conclusions are deferred to Section 6.

2. Statement of the Stefan problem: governing equations and interface conditions

For the sake of simplicity, in the present work we focus on the two-dimensional (2D), steady case; a generalization of our approach to the three-dimensional (3D), time-dependent setting is left for the future. We consider a system consisting of three phases: solid (*S*), liquid (*L*), and gas (*G*), and shown schematically in Fig. 1. The solid and liquid phases are assumed to occupy the domains Ω_S and Ω_L , so that the computational domain is defined as $\Omega_{SL} \triangleq \Omega_S \cup \Omega_L$ (“ \triangleq ” means “equal to by definition”). It is also assumed that the density of the liquid and solid phase is the same. The boundary where the solid domain Ω_S is truncated will be denoted Γ_S and will be assumed fixed. The gas phase will only be treated as “ambient” and will not be explicitly included in our model except for the boundary conditions on the interfaces Γ_{SG} and Γ_{LG} . Our focus will be primarily on determining the position of the interface Γ_{SL} and the contact points *B* and *B'* defined as $\{B, B'\} = \Gamma_{SL} \cap \Gamma_{LG}$. It will be assumed that the interface Γ_{SL} is “structured”, i.e., can be modeled by a surface with zero thickness, whereas the solid–gas and liquid–gas interfaces Γ_{SG} and Γ_{LG} will be assumed flat. The unit normal vectors **n** at the different interfaces are oriented as shown in Fig. 1.

The steady heat transfer is governed by the equations

$$-\nabla \cdot (k_S \nabla T) = 0 \quad \text{in } \Omega_S, \tag{1a}$$

$$-\nabla \cdot (k_L \nabla T) = 0 \quad \text{in } \Omega_L, \tag{1b}$$

where $T \in H^1(\Omega_{SL})$ is the temperature distribution ($H^1(\Omega_{SL})$ is the Sobolev space of functions defined on Ω_{SL} and having square-integrable gradients [18]), whereas k_S and k_L are the thermal diffusivities of the solid and liquid phase, respectively. In our derivations we will allow them to be general functions of *x* and *y*, but in our computations we will assume for simplicity that they are constant and $k_S \neq k_L$. Eq. (1b) are complemented with Neumann-type boundary conditions on the interfaces Γ_{SG} and Γ_{LG}

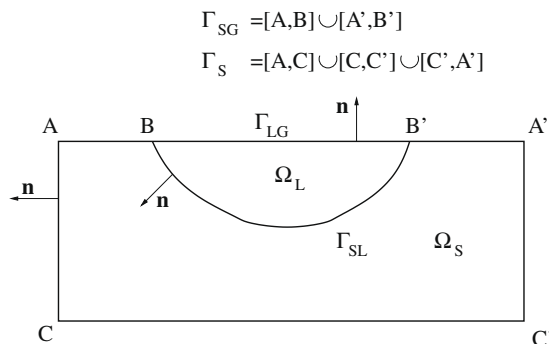


Fig. 1. Schematic of the problem geometry.

$$-k_s \frac{\partial T}{\partial \mathbf{n}} = \varphi_{SG} \quad \text{on } \Gamma_{SG}, \tag{2a}$$

$$-k_L \frac{\partial T}{\partial \mathbf{n}} = \varphi_{LG} \quad \text{on } \Gamma_{LG}, \tag{2b}$$

where φ_{SG} and φ_{LG} are the heat fluxes. On the boundary Γ_S we impose the Dirichlet boundary condition

$$T = T_s \quad \text{on } \Gamma_S, \tag{3}$$

where T_s represents the far-field temperature. We will require that the functions φ_{SG} , φ_{LG} , and T_s be such that they satisfy the compatibility condition (cf. (2a) and (3))

$$-k_s \frac{\partial T_s}{\partial y} = \varphi_{SG} \quad \text{at } A, A', \tag{4}$$

and, in addition, generate single-connected domains Ω_L and Ω_S .

The classical theory of the *steady-state* Stefan problem [19] postulates that the interface Γ_{SL} is fully described by the following two conditions:

(1) Continuous normal heat flux

$$\left[k \frac{\partial T}{\partial \mathbf{n}} \right]_S^L = 0 \quad \text{on } \Gamma_{SL}, \tag{5}$$

where $\left[k \frac{\partial T}{\partial \mathbf{n}} \right]_S^L \triangleq k_L \frac{\partial T}{\partial \mathbf{n}}|_L - k_S \frac{\partial T}{\partial \mathbf{n}}|_S$ with the normal derivatives defined as $\frac{\partial T}{\partial \mathbf{n}}|_S \triangleq \lim_{\epsilon \rightarrow 0} \frac{T(\mathbf{x}_{SL} + \epsilon \mathbf{n}) - T(\mathbf{x}_{SL})}{\epsilon}$ and $\frac{\partial T}{\partial \mathbf{n}}|_L \triangleq \lim_{\epsilon \rightarrow 0} \frac{T(\mathbf{x}_{SL} - \epsilon \mathbf{n}) - T(\mathbf{x}_{SL})}{\epsilon}$; expression (5) represents for some $\mathbf{x}_{SL} \in \Gamma_{SL}$ the jump of the temperature gradient across the interface (in general, $[\cdot]_S^L$ will denote the jump of the given quantity across the interface Γ_{SL}); we note that (5) expresses the conservation of energy known as the first principle of thermodynamics,

(2) Prescribed liquid–solid transition temperature

$$T = \mathcal{T}(\text{interface geometry, material properties}) \quad \text{on } \Gamma_{SL}, \tag{6}$$

where the function $\mathcal{T}(\dots)$ will be specified below; the nature of this condition is more subtle, as it is related to the second principle of thermodynamics which is expressed as an inequality [19]; therefore, as discussed below, condition (6) may take several different thermodynamically consistent forms, and the one employed most commonly is

$$T = T_m \quad \text{on } \Gamma_{SL}, \tag{7}$$

where T_m is a constant melting temperature.

While relations (5) and (7) represent the classical statement of the Stefan interface conditions, many important interfacial phenomena exhibit deviations from the simple relation (7). An extensive review of such phenomena can be found in the monograph [20]. Furthermore, condition (7) is a part of a nonlinear boundary value problem, and as such raises some questions of the mathematical nature. Namely, it follows from this condition that the interface Γ_{SL} must coincide with an isoline of the solution of elliptic problem (1)–(5). In the case when $k_S \neq k_L$ the existence or non-existence of such an isoline is a non-trivial question and can be rigorously established for some simple cases only, see Appendix for a proof of existence for the case when the solution belongs to the Sobolev space $H^2(\Omega_{SL})$, i.e., the space of functions on Ω_{SL} whose second weak derivatives are square-integrable [18]. It is worth noting that although the regularity of harmonic functions on non-smooth domains has been well studied (see, e.g., the monograph [21] and the paper [22]), only few results concern problems in “double-wedge” geometries such as the domain depicted in Fig. 1 (e.g., [23]).

In order to account for situations in which condition (7) may lead to inconsistent formulations, a generalized Stefan condition is derived from the interfacial thermodynamic laws describing the force and energy balances [19]. Let s be the arc-length coordinate along the interface Γ_{SL} and θ the angle between the normal vector \mathbf{n} and the OX axis of the coordinate system, so that $\mathbf{n}(\theta) = [\cos \theta, \sin \theta]^T$. The symbols θ^+ and θ^- will represent the limiting values of the normal angle at the

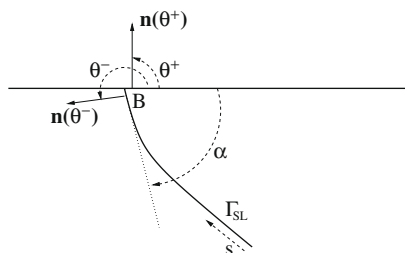


Fig. 2. Neighborhood of the contact point B.

two sides of the contact point B (Fig. 2, the same applies to B'). The tangent vector will be denoted τ . The capillary force \mathbf{C} acting within the interface can be expressed as [19]

$$\mathbf{C}(\theta) = f(\theta)\tau(\theta) + f'(\theta)\mathbf{n}(\theta), \quad (8)$$

where $f(\theta)$ is the interfacial free energy. The analysis carried out in Section 7.4 of [19] yields the following two conditions as a generalization of (7)

$$L \frac{T - T_m}{T_m} = \frac{d\mathbf{C}}{ds} \cdot \mathbf{n} = \kappa \left(f + \frac{d^2 f}{d\theta^2} \right) \quad \text{on the smooth part of } \Gamma_{SL}, \quad (9a)$$

$$\mathbf{C}(\theta^+) \cdot \tau_{LG} = \mathbf{C}(\theta^-) \cdot \tau_{LG} \quad \text{at the contact points } B \text{ and } B', \quad (9b)$$

where L is the latent heat, $\kappa \triangleq d\theta/ds$ is the interface curvature, and τ_{LG} is the vector tangent to the interface Γ_{LG} . As is usually the case in macroscopic models of the Stefan problem, we will assume that the interfacial free energy f is a smooth function of the angle θ . We note in passing that this is not necessarily the case in *microscopic* models which distinguish different grains in the solid material. In such cases the interface Γ_{SL} is a piecewise linear curve with “kinks” corresponding to the grain boundaries which result from the interfacial free energy $f(\theta)$ in the so-called “crystalline form” [19] featuring “cusps” at some particular angles θ . Consequently, $d^2 f/d\theta^2$ may become infinite and the interface should be piecewise flat with each segment characterized by $\kappa = 0$ (called facet) corresponding to one of these singular orientations. The orientation of a facet F is determined from the Herring condition [19]

$$L \int_F \frac{T - T_m}{T_m} ds = \sum_G \frac{f(\theta_F)\tau(\theta_F) \cdot \tau(\theta_G) - \mathbf{C}(\theta_G) \cdot \tau(\theta_G)}{\mathbf{n}(\theta_F) \cdot \tau(\theta_G)}, \quad (10)$$

where G are the facets adjacent to F , θ_G and θ_F are the orientations of the facets G and F , and $\mathbf{C}(\theta_G)$ is the capillary force exerted by the facet G on the facet F . Hence the local condition (9a) is replaced by the nonlocal condition (10) together with the assumption concerning nonsmoothness of f . Details of this formulation can be found in [2], whereas questions of existence and uniqueness of solutions to such problems are studied in [24]. We add that an extension of such formulation to the case involving contact points is not straightforward, and therefore we will not consider this formulation here.

We emphasize that, regardless of the specific form of the boundary condition, both (9b) and (10) involve a new dependent variable, namely, the interfacial free energy f . Therefore, some additional information must be provided in order to determine this quantity and close the system. As a matter of fact, accurate determination of the interfacial free energy f is an extremely difficult task requiring information at the microscopic level which is not usually available in macroscopic computations of the Stefan problem. In many situations involving common materials (e.g., metals) the interfacial energy f is negligibly small which justifies the constant approximation (7), provided the interface is characterized by moderate values of the curvature κ . In the presence of contact points, condition (9b) must be satisfied in addition to (5) and (9a). Consequently, in order to accommodate this additional condition, the right-hand side (RHS) in (9a) must be suitably adjusted, and as a result the constant approximation (7) will no longer apply. Furthermore, we note that condition (9b) determines in fact the *contact angle* α between the interfaces Γ_{SL} and Γ_{LG} at the contact points B and B' (Fig. 2). This is because (9b) represents the balance of the capillary forces acting on the interfaces in the direction of the “translation” of the contact points B and B' . This leads to the known conclusion that the steady-state contact angle α is a constitutive property of the material [19]. Based on these observations, in Section 3 we propose an inverse formulation to resolve this “closure problem”.

3. Inverse model

In this section, we first reformulate the generalized Stefan problem defined by (1)–(5) and (9) as a PDE-constrained optimization (inverse) problem, and then justify this approach as a closure model for unresolved interfacial phenomena. Our attention will be focused on the proper handling of the solution in the neighborhood of the contact points. In Section 2, we argued that imposing a specific contact angle α_m induces a deviation from approximate condition (7). While in principle this deviation is described by the RHS of (9a), it is expressed in terms of a microscopic quantity, the interfacial free energy f , for which no additional equation is readily available. We therefore propose to close system (1)–(5) and (9) by postulating that its solutions exhibit certain macroscopic properties observed in reality. We do this by requiring that the contact angle α at B and B' be approximately equal to α_m . Defining a cost functional in the form

$$\mathcal{J}(\Gamma_{SL}) \triangleq \frac{1}{2} \int_{\Gamma_{SL}} [T(\Gamma_{SL}) - T_m]^2 ds + \frac{\ell}{2} [\cos(\alpha(\Gamma_{SL})) - \cos(\alpha_m)]^2 \Big|_{B, B'}, \quad (11)$$

we state the problem as follows:

$$\min_{\Gamma_{SL}} \mathcal{J}(\Gamma_{SL}), \quad (12)$$

where the dependence of $T(\Gamma_{SL})$ and $\alpha(\Gamma_{SL})$ on the position of the interface Γ_{SL} is expressed through (1)–(5). In contrast to the interfacial free energy f , the positive adjustable parameter ℓ is now a *macroscopic* quantity, as it weighs the deviation from

the prescribed value α_m of the contact angle against a measure of the deviation from approximate condition (7). We also remark that the formulation based on the cosine of the contact angle α is preferable to the formulation based on the angle itself on two counts. Firstly, we notice that $\cos(\alpha) \equiv \boldsymbol{\tau}_{SL} \cdot \boldsymbol{\tau}_{LG}$ where the tangential vectors $\boldsymbol{\tau}_{SL}, \boldsymbol{\tau}_{LG}$ are in fact more readily available in numerical computations than α . Secondly, the formulation based on the cosine is related to Young’s equation frequently arising in capillary physics [20]. It is evident that solutions of problem (11), (12) will depend on the parameter ℓ and one of the goals of this work is to quantify this dependence. To begin with, we review two limiting cases as regards the values of the parameter ℓ . We note that setting $\ell = 0$ removes all constraints on the contact angles, and therefore in this case we can expect an interface Γ_{SL} satisfying condition (7). On the other hand, considering $\ell \rightarrow \infty$ we obtain the case in which the condition $\alpha(\Gamma_{SL}) = \alpha_m$ is enforced in the “hard” sense, i.e., the interface Γ_{SL} will satisfy (9b) exactly. We defer the discussion of the intermediate cases to Section 5. Finally, we add that demonstrating rigorously the existence and uniqueness of solutions of problem (11), (12) is far from trivial and falls beyond the scope of the present work.

We will now show that our proposed approach in fact represents a closure model for unresolved interfacial quantities in system (1)–(5) and (9). In general terms, for a system described by a set of state variables \mathbf{y} satisfying a governing equation $F(\mathbf{y}) = 0$ it is assumed that the state variables are divided into two groups: the resolved quantities \mathbf{y}_0 which are explicitly included in the model, and the unresolved (modeled) quantities \mathbf{y}' . The closure model consists in a relationship $\mathbf{y}' = \mathbf{y}'(\mathbf{y}_0)$ which allows one to express the unresolved quantities in terms of the resolved ones, so that the governing equations can be “closed” as follows $G(\mathbf{y}_0) \triangleq F(\{\mathbf{y}_0, \mathbf{y}'(\mathbf{y}_0)\}) = 0$. We note that our original problem (1)–(5) and (9) is in fact underdetermined, because there is no equation characterizing the interfacial free energy f . Assuming that f is an unresolved quantity, we close the system by replacing Eq. (9a) which involves f with another condition in which f does not appear, namely, (11), (12). This formulation is in fact equivalent to finding an interface Γ_{SL} which is in the mechanical equilibrium. Indeed, we note that the balance of the capillary forces and other forces, including inertia forces, exerted by the crystal and the melt on the interface is given by [19]

$$\frac{d\mathbf{C}}{ds} = \mathbf{n} \cdot \boldsymbol{\sigma}_S - \mathbf{n} \cdot \boldsymbol{\sigma}_L, \tag{13}$$

where $\boldsymbol{\sigma}_S$ and $\boldsymbol{\sigma}_L$ are the stress tensors of the solid and liquid phases. In view of (9a), we observe that minimizing the temperature deviation ($T|_{\Gamma_{SL}} - T_m$) is in fact equivalent to finding an interface which minimizes $(\mathbf{n} \cdot \boldsymbol{\sigma}_S - \mathbf{n} \cdot \boldsymbol{\sigma}_L \cdot \mathbf{n})$ in the mean square sense. This provides a physical justification for the first term in cost functional (11).

Once problem (11), (12) is solved and the position of the interface Γ_{SL} and the interfacial temperature $T|_{\Gamma_{SL}}$ are determined, the unresolved (modeled) quantity f can be determined from system (9b) where the left-hand side in (9a) is already given. Our present investigation is focused solely on the development and validation of a numerical technique for solution of the PDE-constrained optimization problem (11), (12). Problem (9b) can be solved for the interfacial free energy f using standard numerical techniques and this issue will not be addressed here.

4. Solution of the inverse problem

In this section, we propose a gradient-based approach to solution of the inverse problem formulated in Section 3. Local solutions to optimization problems such as (12) are characterized by the first-order optimality conditions which require the Gâteaux differential of the cost functional \mathcal{J} to vanish for all perturbations. In problem (11), (12) the control variable is the position of the interface Γ_{SL} , hence (11), (12) is in fact a *shape optimization* problem. Problems in which the geometry of the domain is an independent variable require special treatment, because this geometry must be suitably parametrized before differentiation with respect to the shape can be meaningfully defined. Such problems can be treated using methods of the shape differential calculus [10], where perturbations of the interface geometry can be represented as

$$\mathbf{x}(t, \mathbf{Z}) = \mathbf{x} + t\mathbf{Z} \quad \text{for } \mathbf{x} \in \Gamma_{SL}(0), \tag{14}$$

where $\Gamma_{SL}(0)$ is the original unperturbed interface and \mathbf{Z} is a “velocity” field defined on Ω_{SL} and characterizing the perturbation. The points $\mathbf{x}(t, \mathbf{Z})$ thus define the perturbed interface $\Gamma_{SL}(t, \mathbf{Z})$ (expressions analogous to (14) could also be written for $\Omega_S(t, \mathbf{Z})$ and $\Omega_L(t, \mathbf{Z})$, but they are omitted here for brevity). We will use the notation $\Omega(0) \triangleq \Omega(0, \mathbf{Z})$ and $\Gamma(0) \triangleq \Gamma(0, \mathbf{Z})$ for domains and interfaces (with suitable subscripts), respectively. The shape differential of a functional such as (11) in the direction of the perturbation field \mathbf{Z} is defined as

$$\mathcal{J}'(\Gamma_{SL}(0); \mathbf{Z}) \triangleq \lim_{t \rightarrow 0} \frac{\mathcal{J}(\Gamma_{SL}(t, \mathbf{Z})) - \mathcal{J}(\Gamma_{SL}(0))}{t}. \tag{15}$$

Given cost functional (11), its shape differential (15) can be computed using a classical result concerning shape differentiation [25] which says that for a smooth domain $\Omega(t, \mathbf{Z})$ and smooth functions f and g defined, respectively, on this domain and its boundary we have

$$\left(\int_{\Omega(t, \mathbf{Z})} f \, d\Omega + \int_{\partial\Omega(t, \mathbf{Z})} g \, ds \right)' = \int_{\Omega(0)} f' \, d\Omega + \int_{\partial\Omega(0)} g' \, ds + \int_{\partial\Omega(0)} \left(f + \boldsymbol{\kappa}g + \frac{\partial g}{\partial n} \right) \mathbf{Z} \cdot \mathbf{n} \, ds, \tag{16}$$

where the prime denotes the shape derivative defined as in (15) and \mathbf{n} is the unit normal vector pointing out of the domain Ω . Since in the present problem the boundary $\partial\Omega_L = \Gamma_{SL} \cup \Gamma_{LG}$ is only Lipschitz continuous, we need the following generalization of the preceding result proved in [19].

Theorem 4.1. *Let g be a smooth function defined on perturbations $\gamma(t, \mathbf{Z})$ of a smooth arc $\gamma(0) \triangleq \gamma(0, \mathbf{Z}) = \widehat{BB'}$. Then*

$$\left(\int_{\gamma(t, \mathbf{Z})} g \, ds \right)' = \int_{\gamma(0)} g' \, ds + \int_{\gamma(0)} \left(\chi g + \frac{\partial g}{\partial \mathbf{n}} \right) \mathbf{Z} \cdot \mathbf{n} \, ds + [g \mathbf{Z} \cdot \boldsymbol{\tau}]_B^{B'}, \tag{17}$$

where $\boldsymbol{\tau}$ is the unit vector tangent to $\gamma(0)$.

We now proceed with differentiation of the second term in (11) involving the contact angle α . By definition, the contact angle α satisfies the relation $\cos(\alpha) = -\boldsymbol{\tau} \cdot \mathbf{e}_x|_{B, B'}$, where \mathbf{e}_x is the unit vector associated with the OX axis, so that using the classical shape differentiation result [10] one obtains

$$[\cos(\alpha)]' = -(\boldsymbol{\tau} \cdot \mathbf{e}_x)' = -\mathbf{n} \cdot \mathbf{e}_x \frac{\partial \mathbf{Z} \cdot \mathbf{n}}{\partial s} = \sin(\alpha) \frac{\partial \mathbf{Z} \cdot \mathbf{n}}{\partial s}, \tag{18}$$

where $\frac{\partial}{\partial s}$ is the gradient in the direction tangential to the interface Γ_{SL} . We are now in the position to compute the complete shape differential of cost functional (11) which yields

$$\begin{aligned} \mathcal{J}'(\Gamma_{SL}(0); \mathbf{Z}) &= \int_{\Gamma_{SL}(0)} (T - T_m) T'|_L + \left[\chi \frac{(T - T_m)^2}{2} + (T - T_m) \frac{\partial T}{\partial \mathbf{n}} \right] \mathbf{Z} \cdot \mathbf{n} \, ds \\ &\quad + \left[\frac{(T - T_m)^2}{2} \mathbf{Z} \cdot \boldsymbol{\tau} + \ell [\cos(\alpha) - \cos(\alpha_m)] \sin(\alpha) \frac{\partial \mathbf{Z} \cdot \mathbf{n}}{\partial s} \right]_B^{B'}, \end{aligned} \tag{19}$$

where $T'|_L$ is the shape derivative of T evaluated on the liquid side of the interface Γ_{SL} . A fundamental result of the shape differential calculus referred to as the “structure theorem” [10] stipulates that the shape differential of a cost functional $\mathcal{J}(\Gamma(0, \mathbf{Z}))$ defined on a closed curve $\Gamma(0, \mathbf{Z})$ can be expressed as

$$\mathcal{J}'(\Gamma(0); \mathbf{Z}) = \int_{\Gamma(0)} h \mathbf{Z} \cdot \mathbf{n} \, ds, \tag{20}$$

where the scalar-valued function h is defined on the curve $\Gamma(0)$. As will be shown later in this section, in our present problem we will need to generalize expression (20) due to the fact that Γ_{SL} is an open arc, rather than a closed curve. In any case, the gradient $\nabla \mathcal{J}$ of the cost functional \mathcal{J} can be extracted by invoking the Riesz theorem [26] to identify the shape differential of $\mathcal{J}(\Gamma_{SL})$ with an inner product as $\mathcal{J}'(\Gamma_{SL}(0); \mathbf{Z}) = \langle \nabla \mathcal{J}, \mathbf{Z} \rangle_{\mathcal{X}(\Gamma_{SL})}$, where $\mathcal{X}(\Gamma_{SL})$ is a Hilbert space of vector-valued functions defined on Γ_{SL} . This gradient is a central element of the following iterative algorithm which can be employed to solve optimization problem (11), (12)

$$\mathbf{x}|_{\Gamma_{SL}^{(k+1)}} = \mathbf{x}|_{\Gamma_{SL}^{(k)}} + \tau_k \mathbf{g}[\nabla \mathcal{J}(\Gamma_{SL}^{(k)})], \quad k = 1, 2, \dots, \tag{21}$$

where $\mathbf{x}|_{\Gamma_{SL}^{(k)}}$ represents the position of the interface Γ_{SL} at the k th iteration and τ_k is the length of the step in the descent direction. The function \mathbf{g} determines the specific form of the optimization algorithm used (e.g., the steepest descent, conjugate gradients, or quasi-Newton method, etc., [27]). We note, however, that expression (19) does not yet have a form compatible with (20), as it explicitly depends on the shape derivative T' . Shape differential (19) can be transformed into a suitable form by introducing the adjoint state $T^* \in H^1(\Omega_{SL})$ and considering the following weak formulation of (1)–(5) in which the adjoint state serves as the test function

$$-\int_{\Omega_L} \nabla \cdot (k_L \nabla T) T^* \, d\Omega - \int_{\Omega_S} \nabla \cdot (k_S \nabla T) T^* \, d\Omega = 0. \tag{22}$$

After integrating by parts and using boundary conditions (2)–(4) we obtain

$$\int_{\Omega_L} k_L (\nabla T \cdot \nabla T^*) \, d\Omega + \int_{\Omega_S} k_S (\nabla T \cdot \nabla T^*) \, d\Omega + \int_{\Gamma_{LG}} T^* \varphi_{LG} \, ds + \int_{\Gamma_{SL}} \left[T^* k \frac{\partial T}{\partial \mathbf{n}} \right]_S^L \, ds + \int_{\Gamma_{SG}} T^* \varphi_{SG} \, ds - \int_{\Gamma_S} k_S T^* \frac{\partial T}{\partial \mathbf{n}} \Big|_S \, ds = 0. \tag{23}$$

We note that before shape differentiation is performed we may not use (5) to simplify the term involving $[T^* k \frac{\partial T}{\partial \mathbf{n}}]_S^L$. Next we apply shape differentiation formulas (16) and (17) to weak formulation (23) which yields

$$\begin{aligned} &\int_{\Omega_L} k_L (\nabla T' \cdot \nabla T^*) \, d\Omega + \int_{\Omega_S} k_S (\nabla T' \cdot \nabla T^*) \, d\Omega + \int_{\Gamma_{LG}} T^* \varphi'_{LG} \, ds - \left(\int_{\Gamma_{SL}(t, \mathbf{Z})} \left[T^* k \frac{\partial T'}{\partial \mathbf{n}} \right]_S^L \, ds \right)' \\ &\quad + \int_{\Gamma_{SG}} T^* \varphi'_{SG} \, ds - \int_{\Gamma_S} k_S T^* \frac{\partial T'}{\partial \mathbf{n}} \Big|_S \, ds + \int_{\Gamma_{SL}} [k \nabla T \cdot \nabla T^*]_S^L \mathbf{Z} \cdot \mathbf{n} \, ds + T^* [(\varphi_{LG} - \varphi_{SG}) \mathbf{Z} \cdot \mathbf{e}_x]_B^{B'} = 0. \end{aligned} \tag{24}$$

Using (17) together with boundary condition (5), the shape differential of the integral over Γ_{SL} can be expressed as

$$\left(\int_{\Gamma_{SL}(t; \mathbf{Z})} \left[T^* k \frac{\partial T}{\partial \mathbf{n}} \right]_S^L ds \right)' = \int_{\Gamma_{SL}(0)} \frac{\partial}{\partial \mathbf{n}} \left[T^* k \frac{\partial T}{\partial \mathbf{n}} \right]_S^L \mathbf{Z} \cdot \mathbf{n} ds = \int_{\Gamma_{SL}(0)} \left[k \frac{\partial T}{\partial \mathbf{n}} \frac{\partial T^*}{\partial \mathbf{n}} \right]_S^L \mathbf{Z} \cdot \mathbf{n} ds, \tag{25}$$

where we used the fact that $\varphi_{SL} \triangleq [k \frac{\partial T}{\partial \mathbf{n}}]_S^L = 0$ on Γ_{SL} , so that φ_{SL} admits an extension with zero into the domains Ω_S and Ω_L . Using this result in (24) and performing integration by parts one more time leads to

$$\begin{aligned} & - \int_{\Omega_L} \nabla \cdot (k_L \nabla T^*) T' d\Omega - \int_{\Omega_S} \nabla \cdot (k_S \nabla T^*) T' d\Omega + \int_{\Gamma_{SL}} \left[k T' \frac{\partial T^*}{\partial \mathbf{n}} \right]_S^L ds + \int_{\Gamma_{LG}} \left(k_L T' \frac{\partial T^*}{\partial \mathbf{n}} \Big|_L + T^* \varphi'_{LG} \right) ds \\ & - \int_{\Gamma_{SL}} \left[k \frac{\partial T^*}{\partial \mathbf{n}} \frac{\partial T}{\partial \mathbf{n}} \right]_S^L \mathbf{Z} \cdot \mathbf{n} ds + \int_{\Gamma_{SG}} \left(k_S T' \frac{\partial T^*}{\partial \mathbf{n}} \Big|_S + T^* \varphi'_{SG} \right) ds + \int_{\Gamma_S} k_S \left(T' \Big|_S \frac{\partial T^*}{\partial \mathbf{n}} \Big|_S - T^* \frac{\partial T'}{\partial \mathbf{n}} \Big|_S \right) ds \\ & + \int_{\Gamma_{SL}} [k \nabla T \cdot \nabla T^*]_S^L \mathbf{Z} \cdot \mathbf{n} ds + T^* [(\varphi_{LG} - \varphi_{SG}) \mathbf{Z} \cdot \mathbf{e}_x]_B^B = 0. \end{aligned} \tag{26}$$

We remark that the shape derivative field T' is discontinuous across the interface Γ_{SL} . Shape differentiation of boundary condition (3) and of the relationship $T|_S = T|_L$ expressing the continuity of the temperature field across the interface Γ_{SL} yields [25]

$$T' = 0 \quad \text{on } \Gamma_S, \tag{27}$$

$$[T']_S^L + \left[\frac{\partial T'}{\partial \mathbf{n}} \right]_S^L \mathbf{Z} \cdot \mathbf{n} = 0 \quad \text{on } \Gamma_{SL}. \tag{28}$$

We assume that the functions φ_{SG} and φ_{LG} appearing in boundary conditions (2a) and (2b) are invariant with respect to perturbations of the domain given by \mathbf{Z} , so that

$$\varphi'_{SG} \equiv 0, \tag{29a}$$

$$\varphi'_{LG} \equiv 0. \tag{29b}$$

Let us now suppose that the adjoint state T^* satisfies the following equations

$$-\nabla \cdot (k_S \nabla T^*) = 0 \quad \text{in } \Omega_S, \tag{30a}$$

$$-\nabla \cdot (k_L \nabla T^*) = 0 \quad \text{in } \Omega_L, \tag{30b}$$

with the boundary conditions

$$-\left[k \frac{\partial T^*}{\partial \mathbf{n}} \right]_S^L = T - T_m \quad \text{on } \Gamma_{SL}, \tag{31}$$

$$-k_S \frac{\partial T^*}{\partial \mathbf{n}} = 0 \quad \text{on } \Gamma_{SG}, \tag{32}$$

$$-k_L \frac{\partial T^*}{\partial \mathbf{n}} = 0 \quad \text{on } \Gamma_{LG}, \tag{33}$$

$$T^* = 0 \quad \text{on } \Gamma_S. \tag{34}$$

Using relations (27) and (28) together with the definition of the adjoint system in (30)–(34) allows us to simplify expression (26), so that we obtain

$$\begin{aligned} & \int_{\Gamma_{SL}} \left[- \left(T' \Big|_L + \frac{\partial T'}{\partial \mathbf{n}} \Big|_L \mathbf{Z} \cdot \mathbf{n} \right) (T - T_m) - \left[k \frac{\partial T}{\partial \mathbf{n}} \frac{\partial T^*}{\partial \mathbf{n}} \right]_S^L \mathbf{Z} \cdot \mathbf{n} \right] ds + \int_{\Gamma_{SL}} \left([k \nabla T \cdot \nabla T^*]_S^L - \left[k \frac{\partial T}{\partial \mathbf{n}} \frac{\partial T^*}{\partial \mathbf{n}} \right]_S^L \right) \mathbf{Z} \cdot \mathbf{n} ds \\ & + T^* [(\varphi_{LG} - \varphi_{SG}) \mathbf{Z} \cdot \mathbf{e}_x]_B^B = 0, \end{aligned} \tag{35}$$

where we also used the equality

$$\left[k T' \frac{\partial T^*}{\partial \mathbf{n}} \right]_S^L = \left(T' \Big|_L + \frac{\partial T'}{\partial \mathbf{n}} \Big|_L \mathbf{Z} \cdot \mathbf{n} \right) \left[k \frac{\partial T^*}{\partial \mathbf{n}} \right]_S^L - \left[k \frac{\partial T}{\partial \mathbf{n}} \frac{\partial T^*}{\partial \mathbf{n}} \right]_S^L \mathbf{Z} \cdot \mathbf{n}, \tag{36}$$

which is a consequence of (28). After further simplifications and regrouping certain terms (35) becomes

$$\int_{\Gamma_{SL}} \left(\left[k \frac{\partial T}{\partial \mathbf{s}} \frac{\partial T^*}{\partial \mathbf{s}} \right]_S^L - \left[k \frac{\partial T}{\partial \mathbf{n}} \frac{\partial T^*}{\partial \mathbf{n}} \right]_S^L \right) \mathbf{Z} \cdot \mathbf{n} ds + T^* [(\varphi_{LG} - \varphi_{SG}) \mathbf{Z} \cdot \mathbf{e}_x]_B^B = \int_{\Gamma_{SL}} (T - T_m) \left(T' \Big|_L + \frac{\partial T'}{\partial \mathbf{n}} \Big|_L \mathbf{Z} \cdot \mathbf{n} \right) ds, \tag{37}$$

where we used the fact that $\nabla T = \frac{\partial T}{\partial \mathbf{n}} \mathbf{n} + \frac{\partial T}{\partial \mathbf{s}} \boldsymbol{\tau}$. One recognizes that the terms on the RHS in (37) also appear in expression (19) for the shape differential $\mathcal{J}'(\Gamma_{SL}(0); \mathbf{Z})$, so that (37) can be used to eliminate T' from this expression which gives

$$\begin{aligned} \mathcal{J}'(\Gamma_{SL}(0); \mathbf{Z}) &= \int_{\Gamma_{SL}} \left(\left[k \frac{\partial T}{\partial s} \frac{\partial T^*}{\partial s} \right]_s^L - \left[k \frac{\partial T}{\partial n} \frac{\partial T^*}{\partial n} \right]_s^L + \kappa \frac{(T - T_m)^2}{2} \right) \mathbf{Z} \cdot \mathbf{n} ds + \left[T^*(\varphi_{LG} - \varphi_{SG}) \mathbf{Z} \cdot \mathbf{e}_x + \frac{\mathbf{Z}}{\cdot} \tau \right]_B^{B'} \\ &+ \ell [\cos(\alpha) - \cos(\alpha_m)] \sin(\alpha) \left(\kappa \mathbf{Z} \cdot \boldsymbol{\tau} + \frac{\partial \mathbf{Z}}{\partial s} \cdot \mathbf{n} \right) \Big|_B^{B'}. \end{aligned} \tag{38}$$

We note that, since \mathbf{Z} appears explicitly in (38), this expression of the cost differential is now consistent with the Riesz theorem and (20), and can be employed to identify the cost functional gradient. For example, choosing $L^2(\Gamma_{SL})$ as the function space $\mathcal{X}(\Gamma_{SL})$ in Riesz identity, we identify expression (38) with an L^2 inner product as $\mathcal{J}'(\Gamma_{SL}(0); \mathbf{Z}) = \langle \nabla^{L^2} \mathcal{J}, \mathbf{Z} \rangle_{L^2(\Gamma_{SL})}$, so that we obtain

$$\begin{aligned} \nabla^{L^2} \mathcal{J} &= \left[\left[k \frac{\partial T}{\partial s} \frac{\partial T^*}{\partial s} \right]_s^L - \left[k \frac{\partial T}{\partial n} \frac{\partial T^*}{\partial n} \right]_s^L + \kappa \frac{(T - T_m)^2}{2} \right] \mathbf{n} \\ &+ \left[T^*(\varphi_{LG} - \varphi_{SG}) \mathbf{e}_x + \frac{(T - T_m)^2}{2} \boldsymbol{\tau} + \kappa \ell [\cos(\alpha) - \cos(\alpha_m)] \sin(\alpha) \boldsymbol{\tau} \right] [\delta(s - s_{B'}) - \delta(s - s_B)] \\ &+ \ell [\cos(\alpha) - \cos(\alpha_m)] \sin(\alpha) [\dot{\delta}(s - s_{B'}) - \dot{\delta}(s - s_B)] \mathbf{n} \quad \text{on } \Gamma_{SL}, \end{aligned} \tag{39}$$

where s_B and $s_{B'}$ are the arc-length coordinates of the contact points B and B' , whereas $\dot{\delta}$ represents the distributional derivative of the Dirac delta. It arises through integration by parts with respect to s of the terms defined at the contact points B and B' . We note that the gradient $\nabla^{L^2} \mathcal{J}$, being a vector-valued function defined on the interface Γ_{SL} , has components in both the direction normal and tangential to the interface, which might appear to contradict the “structure theorem” as expressed in (20). The reason for this discrepancy is that derivation of (20) supposes the interface to be a closed, smooth manifold, so that the tangential terms never arise. As is evident from (39), the tangential component of the gradient $\nabla^{L^2} \mathcal{J}$ is localized at the contact points B and B' only. Hence, this component can be interpreted as locally “stretching” the interface Γ_{SL} so that the contact points stay at the top surface $\Gamma_{SG} \cup \Gamma_{LG}$ when the interface Γ_{SL} is displaced in the normal direction \mathbf{n} . We also note that, owing to the presence of the Dirac delta terms δ and their distributional derivatives $\dot{\delta}$ localized at B and B' , the L^2 gradient given in (39) is a very non-smooth distribution. While L^2 gradients are the most common choice in adjoint-based optimization of PDE systems [28], they are clearly inapplicable in the present problem. The reason is that the interface cannot be displaced in a discontinuous manner, as this would be inconsistent with the continuity of the medium. We will solve this problem by imposing some smoothness requirements on the gradient and to simplify the derivation we introduce the quantity $\mathbf{e}_r \triangleq \frac{\mathbf{r}}{|\mathbf{r}|}$, where $\mathbf{r} \triangleq [x, y]^T$ is the position vector determined with respect to an origin located on the boundary segment Γ_{LG} . We will restrict our attention to the perturbation fields in the form $\mathbf{Z} = \zeta \mathbf{e}_r$, where ζ is a scalar function defined on the interface Γ_{SL} . We note that since $\zeta \mathbf{e}_r$ is tangential to $\Gamma_{SG} \cup \Gamma_{LG}$ at B and B' , the tangential component of the gradient is not required to keep the contact points on this boundary segment. The Riesz identity now becomes

$$\mathcal{J}'(\Gamma_{SL}(0); \mathbf{Z}) = \langle \nabla^{\mathcal{X}} \mathcal{J}, \mathbf{Z} \rangle_{\mathcal{X}(\Gamma_{SL})} = \langle \nabla^{\mathcal{X}} \mathcal{J}, \zeta \mathbf{e}_r \rangle_{\mathcal{X}(\Gamma_{SL})} = \langle \mathbf{e}_r \cdot \nabla^{\mathcal{X}} \mathcal{J}, \zeta \rangle_{\tilde{\mathcal{X}}(\Gamma_{SL})} = \langle \nabla_r^{\mathcal{X}} \mathcal{J}, \zeta \rangle_{\tilde{\mathcal{X}}(\Gamma_{SL})} = \mathcal{J}'(\Gamma_{SL}(0); \zeta), \tag{40}$$

where we denoted $\nabla_r^{\mathcal{X}} \mathcal{J} \triangleq \mathbf{e}_r \cdot \nabla^{\mathcal{X}} \mathcal{J}$ the radial component of the gradient which is a scalar function, and $\tilde{\mathcal{X}}(\Gamma_{SL})$ is the Hilbert space of scalar functions defined on Γ_{SL} . We now require that this gradient should belong to the Sobolev space $H^2(\Gamma_{SL})$ with the inner product defined as

$$\langle u, v \rangle_{H^2(\Gamma_{SL})} = \int_{\Gamma_{SL}} \left(uv + l_1^2 \frac{\partial u}{\partial s} \frac{\partial v}{\partial s} + l_2^4 \frac{\partial^2 u}{\partial s^2} \frac{\partial^2 v}{\partial s^2} \right) ds = \int_{\Gamma_{SL}} \left(u - l_1^2 \frac{\partial^2 u}{\partial s^2} + l_2^4 \frac{\partial^4 u}{\partial s^4} \right) v ds + \left(l_1^2 \frac{\partial u}{\partial s} - l_2^4 \frac{\partial^3 u}{\partial s^3} \right) v \Big|_B^{B'} + l_2^4 \frac{\partial^2 u}{\partial s^2} \frac{\partial v}{\partial s} \Big|_B^{B'}, \tag{41}$$

where $u, v \in H^2(\Gamma_{SL})$ and l_1 and l_2 are adjustable parameters with the meaning of a length-scale. Choosing $H^2(\Gamma_{SL})$ as the space $\tilde{\mathcal{X}}(\Gamma_{SL})$ in the Riesz identity, one can identify expression (38) with an H^2 inner product (41) as $\mathcal{J}'(\Gamma_{SL}(0); \zeta) = \langle \nabla_r^{H^2} \mathcal{J}, \zeta \rangle_{H^2(\Gamma_{SL})}$. In view of the arbitrariness of ζ we obtain

$$\nabla_r^{H^2} \mathcal{J} - l_1^2 \frac{\partial^2 \nabla_r^{H^2} \mathcal{J}}{\partial s^2} + l_2^4 \frac{\partial^4 \nabla_r^{H^2} \mathcal{J}}{\partial s^4} = \left[\left[k \frac{\partial T}{\partial s} \frac{\partial T^*}{\partial s} \right]_s^L - \left[k \frac{\partial T}{\partial n} \frac{\partial T^*}{\partial n} \right]_s^L + \kappa \frac{(T - T_m)^2}{2} \right] \mathbf{n} \cdot \mathbf{e}_r \quad \text{on } \Gamma_{SL}, \tag{42a}$$

$$l_1^2 \frac{\partial \nabla_r^{H^2} \mathcal{J}}{\partial s} - l_2^4 \frac{\partial^3 \nabla_r^{H^2} \mathcal{J}}{\partial s^3} = T^*(\varphi_{LG} - \varphi_{SG}) \mathbf{e}_x \cdot \mathbf{e}_r + \frac{(T - T_m)^2}{2} \boldsymbol{\tau} \cdot \mathbf{e}_r + \ell \kappa [\cos(\alpha) - \cos(\alpha_m)] \sin(\alpha) \boldsymbol{\tau} \cdot \mathbf{e}_r \quad \text{at } B, B', \tag{42b}$$

$$l_2^4 \frac{\partial^2 \nabla_r^{H^2} \mathcal{J}}{\partial s^2} = \ell [\cos(\alpha) - \cos(\alpha_m)] \sin(\alpha) \mathbf{n} \cdot \mathbf{e}_r \quad \text{at } B, B'. \tag{42c}$$

Thus, the $\nabla_r^{H^2} \mathcal{J}$ gradient can be determined by solving a fourth-order boundary value problem defined on the interface Γ_{SL} . In order to avoid certain technicalities related to solution of this problem in practice, our computational results reported in

Section 5 will correspond to the limit $l_2 \rightarrow 0$ in which the terms with the highest derivatives in (42c) vanish, and instead of an H^2 gradient we obtain an H^1 gradient defined by a system with the Helmholtz operator

$$\nabla_{\mathbf{r}}^{H^1} \mathcal{J} - l_1^2 \frac{\partial^2 \nabla_{\mathbf{r}}^{H^1} \mathcal{J}}{\partial s^2} = \left[\left[k \frac{\partial T}{\partial s} \frac{\partial T^*}{\partial s} \right]_S^L - \left[k \frac{\partial T}{\partial n} \frac{\partial T^*}{\partial n} \right]_S^L + \varkappa \frac{(T - T_m)^2}{2} \right] \mathbf{n} \cdot \mathbf{e}_{\mathbf{r}} \quad \text{on } \Gamma_{SL}, \tag{43a}$$

$$l_1^2 \frac{\partial \nabla_{\mathbf{r}}^{H^1} \mathcal{J}}{\partial s} = T^* (\varphi_{LG} - \varphi_{SG}) \mathbf{e}_x \cdot \mathbf{e}_{\mathbf{r}} + \frac{(T - T_m)^2}{2} \boldsymbol{\tau} \cdot \mathbf{e}_{\mathbf{r}} + \ell \varkappa [\cos(\alpha) - \cos(\alpha_m)] \sin(\alpha) \boldsymbol{\tau} \cdot \mathbf{e}_{\mathbf{r}} \quad \text{at } B, B'. \tag{43b}$$

We add that taking the limit $l_2 \rightarrow 0$ in (42c) is in fact equivalent to neglecting the terms involving $\frac{\partial \varepsilon}{\partial s} \cdot \mathbf{n}$ in (38). In the context of adjoint-based PDE-constrained optimization, an approach involving H^1 gradients was investigated in [29], where it was shown that the inverse Helmholtz operator is in fact a low-pass filter with the cut-off proportional to l_1^{-1} , so that the parameter l_1 can be used to control the smoothness of the gradient $\nabla_{\mathbf{r}}^{H^1} \mathcal{J}$. For a general overview of Sobolev gradients we refer the reader to the monograph [30]. We add that some of the results presented here were computed using both the H^1 and H^2 gradients and in each case the gain from using the H^2 gradient was rather insignificant (on average, less than 5% in terms of the value of the cost functional at any iteration). We finally remark that assuming the boundary perturbation in the form $\mathbf{Z} = \zeta \mathbf{e}_{\mathbf{r}}$, and therefore working with the gradient defined as a scalar function, significantly simplifies determination of the Sobolev gradients, because one does not have to differentiate the unit vectors $\mathbf{n}(s)$ and $\boldsymbol{\tau}(s)$ in (41).

5. Computational results

In this section, we present numerical results illustrating performance of the proposed method in the following test cases:

- (1) (Case A) no conditions on the contact angles at B and B' , i.e., $\ell = 0$ in (11), which is equivalent to neglecting condition (9b); this case will serve as a reference,
- (2) (Case B) contact angle α_m prescribed at B , but not at B' ,
- (3) (Case C) system (1)–(5) considered in a moving frame of reference with no conditions imposed on the contact angles B and B' ; this case may serve as an approximate model of a welding process in the steady-state regime.

Before discussing the results for each of these cases in detail, we review some diagnostics concerning the determination of the cost functional gradients and the convergence of the iterations. In terms of iterative process (21) we employ the conjugate gradient method to determine the descent direction \mathbf{g} combined with a line minimization to determine the length of the step τ_k [27]. This algorithm is implemented as follows (“ \leftarrow ” denotes assignment):

```

k ← 1
ΓSL(1) ← initial guess
repeat
  solve direct problem (1)–(5)
  solve adjoint problem (30)–(34)
  solve (43b) to determine ∇rH1 J(ΓSL(k))
  perform line minimization minτ J(χ|ΓSL(k) + τg(k)) to find the step-size τk
  deform ΓSL along the conjugate direction g[∇rH1 J(ΓSL(k))] with the step size τk,
  if |J(ΓSL(k+1)) - J(ΓSL(k))| <  $\frac{\varepsilon_J}{2} (|J(ΓSL(k+1))| + |J(ΓSL(k))| + \varepsilon_a)$  then
    l1 ← max(l1/2, εl)
  end if
  k ← k + 1
until |τk| < ετ
    
```

where $\varepsilon_J, \varepsilon_a, \varepsilon_l$ and ε_τ are different adjustable tolerances. We note that the length-scale l_1 is adaptively decreased in the course of the iterations, so that the H^1 gradients gradually approach L^2 gradients for increasing k . The initial guesses $\Gamma_{SL}^{(1)}$ in cases A and C are chosen as arcs with some arbitrary shape, whereas in case B it is taken as the solution $\Gamma_{SL}^{(\infty)}$ obtained in case A. We note that optimization problem (11), (12) is nonconvex and, in principle, different local minimizers can be obtained from different initial guesses. While the presence of such nonunique solutions was indeed observed in some of our computations, we made sure that the results presented in this section belong to the same family of solutions (parameterized by α_m and ℓ). The thermal diffusivities are selected as $k_S = 200$ and $k_L = 100$. Since our mathematical model intends to represent a simplified weld pool created during a welding process, we choose boundary conditions (2a) and (2b) on the top surface to represent the heat flow into the weld pool, i.e.,

$$\varphi_G = \begin{cases} \varphi_{SG} & \text{on } \Gamma_{SG} \\ \varphi_{LG} & \text{on } \Gamma_{LG} \end{cases} \triangleq \begin{cases} 20 & \text{if } |x| > 0.5, \\ 2 \cdot 10^3 \text{ hat}_{0,1}(x) + 20 & \text{if } |x| \leq 0.5, \end{cases} \tag{44}$$

where $\text{hat}_{x_0, m_{\text{sup}}}(x)$ is a smoothed version of the hat function centered at the point x_0 with the support of measure m_{sup} (smoothing is applied so that the second derivative is continuous). Both the direct and the adjoint problem were solved using the finite element method (FEM) on an unstructured, locally-refined mesh which was implemented in the multiphysics modeling environment COMSOL [31], where additional subroutines were developed by the authors to handle the optimization algorithm. The discretization points for the free boundary Γ_{SL} were chosen among the finite element mesh points (finer resolution was not necessary, as the gradient accuracy is ultimately limited by the accuracy of the solution of the direct problem). A cubic spline interpolation was used to define the displacement in all other points on the free boundary.

We begin presentation of our results with a test showing consistency of the gradient computations. To fix attention, we focus on case A. In the spirit of [32], we define the quantity

$$\kappa(\varepsilon) = \frac{\varepsilon^{-1} [\mathcal{J}(\Gamma_{SL}(\varepsilon, \zeta)) - \mathcal{J}(\Gamma_{SL}(0))] }{\langle \nabla_{\mathbf{r}}^x \mathcal{J}, \zeta \rangle_x}, \tag{45}$$

where the numerator is a finite-difference approximation of the Gâteaux shape differential $\mathcal{J}'(\Gamma_{SL}(0); \zeta)$ computed for some perturbation ζ , whereas the denominator expresses this differential in terms of the adjoint field. Thus, deviation of $\kappa(\varepsilon)$ from unity is a measure of the inconsistency of the gradient. In Fig. 3, we observe that the quantity $\kappa(\varepsilon)$ is indeed very close to the unity for different perturbations ζ when the magnitude ε of the perturbation varies over almost three orders of magnitude. Deviation of $\kappa(\varepsilon)$ from the unity observed for very small values of ε is the result of the round-off (subtractive cancellation) errors, whereas the deviations observed for large values of ε are due to truncation errors (loss of validity of the linear approximation). We remark that in such tests one cannot apply perturbations whose support is not entirely contained in Γ_{SL} which is due to the presence of singular terms in (38) with the magnitude of the singularity depending on the contact angle. We also emphasize that since we use here the “differentiate-then-discretize” rather than “discretize-then-differentiate” approach, the gradient should not be expected to be accurate up to the machine precision [28].

Convergence of iterations is shown in Fig. 4 where we illustrate the decrease of the cost functional $\mathcal{J}(\Gamma_{SL}^{(k)})$ with the iterations k . We note a rapid decrease, by about eight orders of magnitude, occurring over 80 iterations. For comparison, we also illustrate the convergence of an iterative process using gradients with the “contact point term” [i.e., the second term on the RHS in (42b)] omitted. Such “contact point terms” are present in the boundary conditions defining the gradient even if no constraints are imposed on the contact angles at B and B' [see the last term in (17)]. A noticeably slower convergence observed in this case underlines the importance of such “contact point terms”. In Fig. 5a and b we show the deviation of the interface temperature $T|_{\Gamma_{SL}}$ from the melting temperature T_m together with the corresponding gradient at the different iterations. As expected, in the case with no constraints on the contact angle, we observe that the interface temperature $T|_{\Gamma_{SL}}$ gradually settles at the constant value T_m everywhere along the interface, so that $(T|_{\Gamma_{SL}^{(k)}} - T_m) \rightarrow 0$ as $k \rightarrow \infty$. In fact, in Appendix we prove that in problems with no constraints on the contact angles free boundaries coincide with temperature isolines. We conclude the discussion of case A by showing in Fig. 6 the temperature isolines together with the position of the interface Γ_{SL} in a converged solution.

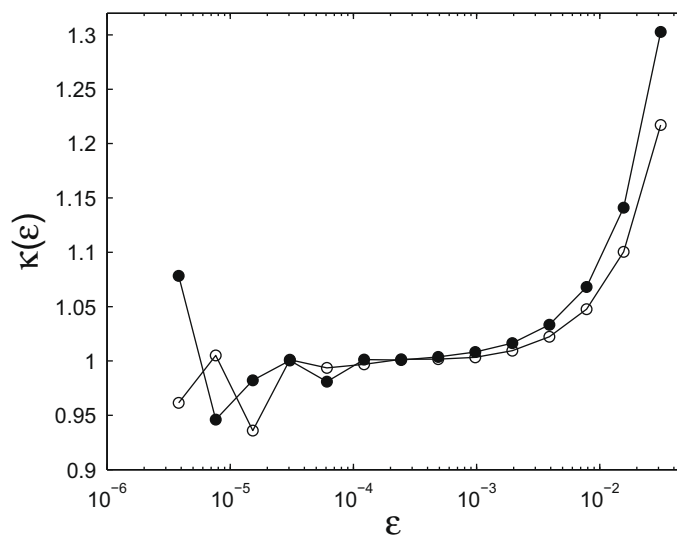


Fig. 3. Dependence of the quantity κ [cf. (45)] on ε . The perturbation ζ is a piecewise linear function of the arc-length coordinate coinciding with a finite element basis function with the support contained in Γ_{SL} : (empty symbols) perturbation adjacent to the contact point B and (solid symbols) perturbation far from the contact points.

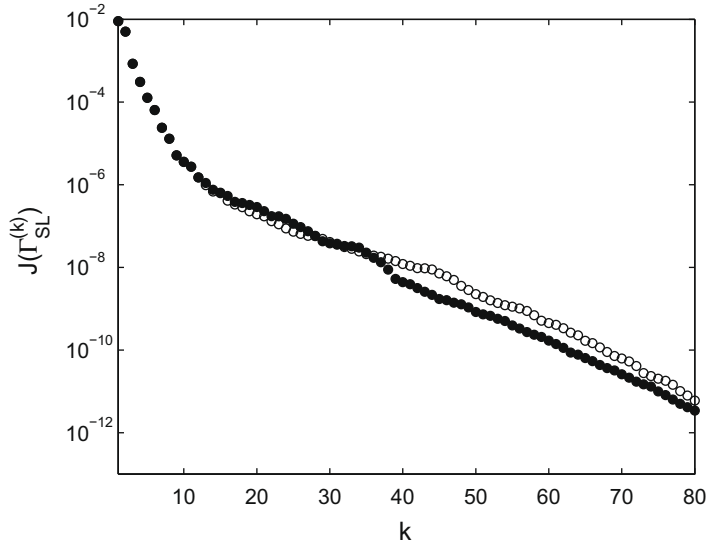


Fig. 4. Cost functional $\mathcal{J}(\Gamma_{SL}^k)$ as a function of the iteration count k using (solid symbols) complete gradients defined in (43b), and (empty symbols) incomplete gradients with the “contact point terms” omitted.

Next we consider case B in which we prescribe the contact angle and compare the results to the case with no constraints on the contact angle. For comparison purposes, the contact angle is prescribed at the left contact point B only. The problem with an imposed contact angle is more delicate, therefore we present our results for this case in greater detail. We will first show results corresponding to $\ell = 10^{-2}$ which is a rather large value of this parameter and ensures that the effect of the fixed contact angle can be detected over relatively large distances from the contact point. In the sequel we will also consider the problem for a range of different values of ℓ . We begin by investigating the convergence of the solutions to problem (11), (12) with respect to grid refinement. The grid is refined in the neighborhood of the contact point only using standard tools available in COMSOL. In this numerical experiment we find interfaces corresponding to four successive grid refinements with the average grid size around the contact point given by $h = \{5 \times 10^{-6}, 5 \times 10^{-5}, 5 \times 10^{-4}, 5 \times 10^{-3}\}$. In each of these cases the average grid size away from the contact points is the same and equal to $h_0 = 5 \times 10^{-3}$. We analyze convergence by examining the position of the interface obtained for different numerical resolutions h and related to the best resolved computation, i.e., using the quantity

$$\xi^h(s) \triangleq |[\mathbf{x}^h(s) - \mathbf{x}_{\text{ref}}(s)] \cdot \mathbf{n}_{\text{ref}}(s)| \quad \mathbf{x}^h \in \Gamma_{SL}^h, \mathbf{x}_{\text{ref}} \in \Gamma_{SL}, \tag{46}$$

where the objects with the superscript “ h ” are computed with the corresponding resolution, whereas the objects with the subscript “ref” correspond to the reference (finest) resolution $h_{\text{ref}} = 10^{-6}$. The parametrization of the curve Γ_{SL}^h with s is defined in such a way that for every s the point $\mathbf{x}^h(s)$ is at the intersection of $\mathbf{n}_{\text{ref}}(s)$ and Γ_{SL}^h . The results of the convergence study are presented in Fig. 7 where we show $\xi^h(s)$ for different values of h . In this Figure we note the systematic decrease of the error ξ^h for all s as the mesh size is refined. Remarkably, while the mesh refinement takes place in the vicinity of the contact point only, the errors are reduced globally over the entire interface Γ_{SL} . In view of these rather small errors, unless stated otherwise, in the subsequent tests we will use the mesh size $h = h_0 = 5 \times 10^{-3}$.

Next, Fig. 8 illustrates the deviation of the interface temperature $T|_{\Gamma_{SL}}$ from the constant value T_m as the contact angle α_m deviates from approx. 64° which was the angle obtained in case A, i.e., without any constraints. Since the deviation $T|_{\Gamma_{SL}} - T_m$ is quite localized near the contact point B , in Fig. 8a we employ a logarithmic scale for the coordinate s which allows us to represent the entire interface Γ_{SL} in the figure. We notice that changes of the imposed contact angle do not globally affect the solution and the observed deviations of $T|_{\Gamma_{SL}} - T_m$ from zero are local and grow as the contact angle decreases. It is also visible that the magnitude of this deviation depends on how the prescribed contact angle differs from the value obtained with no constraints. The local (in space) nature of this effect is also observed in Fig. 9 where we present the interfaces Γ_{SL} obtained as solutions of the optimization problems corresponding to different values of the contact angle α_m prescribed at B .

It was mentioned in Section 3 that the parameter ℓ appearing in definition (11) of the cost functional has the meaning of the inverse of relative variation of the length-scale characterizing the distance from the contact point where condition (9a) significantly deviates from (7). This effect is clearly visible in Fig. 10 in which we show how the absolute value of the deviation of $T(s)|_{\Gamma_{SL}}$ from T_m varies with the distance s from the contact point for different values of the parameter ℓ . We observe that with an increase of ℓ the deviation $|T(s)|_{\Gamma_{SL}} - T_m$ vanishes much faster with s , but its magnitude at $s = 0^+$ increases. In other words, the deviation becomes much more localized for large values of ℓ . There is arguably a universal pattern discernible in Fig. 10, and by quantifying this pattern we will attempt to reveal the intrinsic nature of the parameter ℓ . As regards

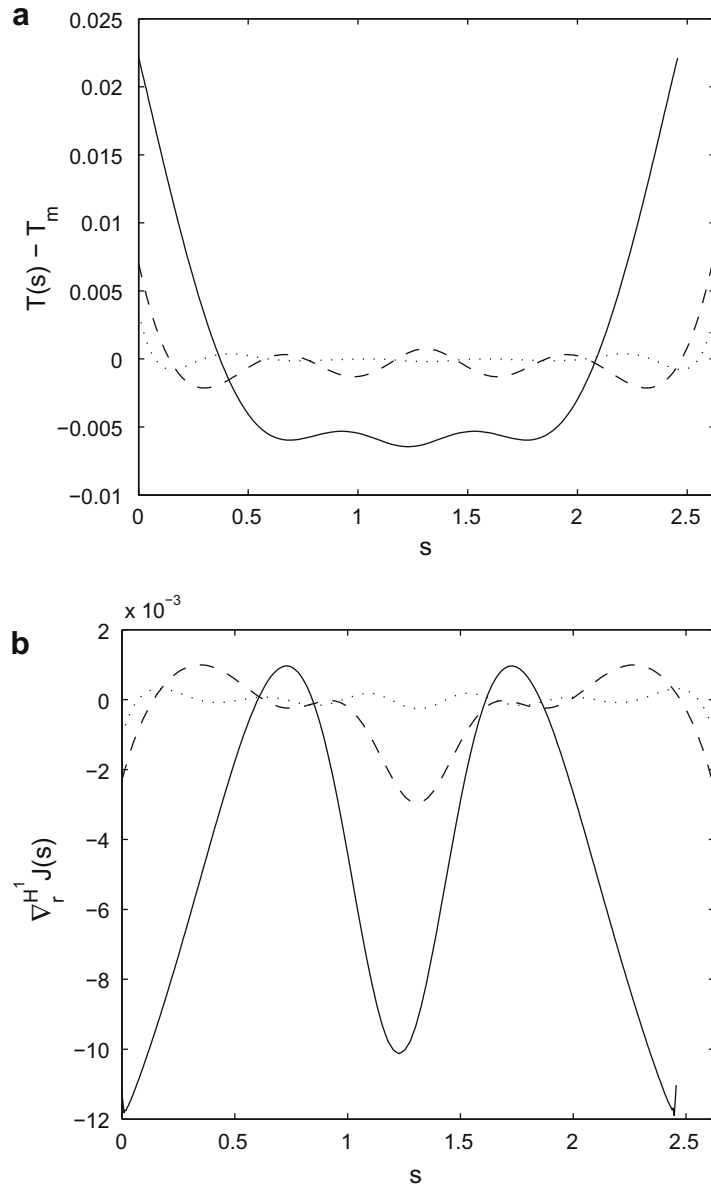


Fig. 5. (a) Deviations of the interface temperature $T|_{\Gamma_{SL}}$ from T_m , and (b) the H^1 gradients of the cost functional $\mathcal{J}(\Gamma_{SL})$ along the interface Γ_{SL} at (solid line) the 5th iteration, (dashed line) 10th iteration, and (dotted line) 20th iteration.

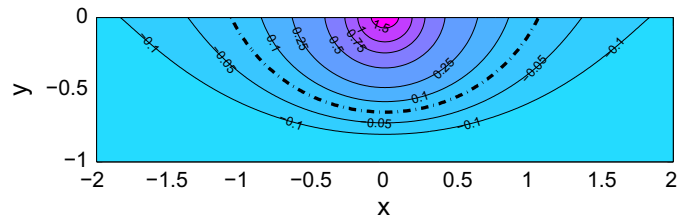


Fig. 6. Temperature isolines $T(x,y) - T_m$ and (dashed line) the interface Γ_{SL} in the solution of the problem in case A.

characterizing the distance from the contact point where the deviation $|T(s)|_{\Gamma_{SL}} - T_m|$ is significant, there are many different possibilities and, to fix attention, we will consider the following two quantities

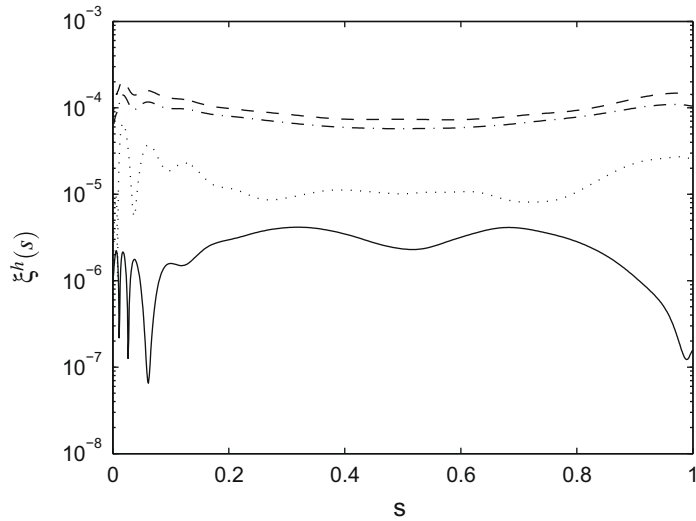


Fig. 7. Analysis of convergence with respect to mesh refinement using the displacement ξ^h for (solid) $h = 5 \times 10^{-6}$, (dotted) $h = 5 \times 10^{-5}$, (dash-dotted) $h = 5 \times 10^{-4}$, (dashed) $h = 5 \times 10^{-3}$.

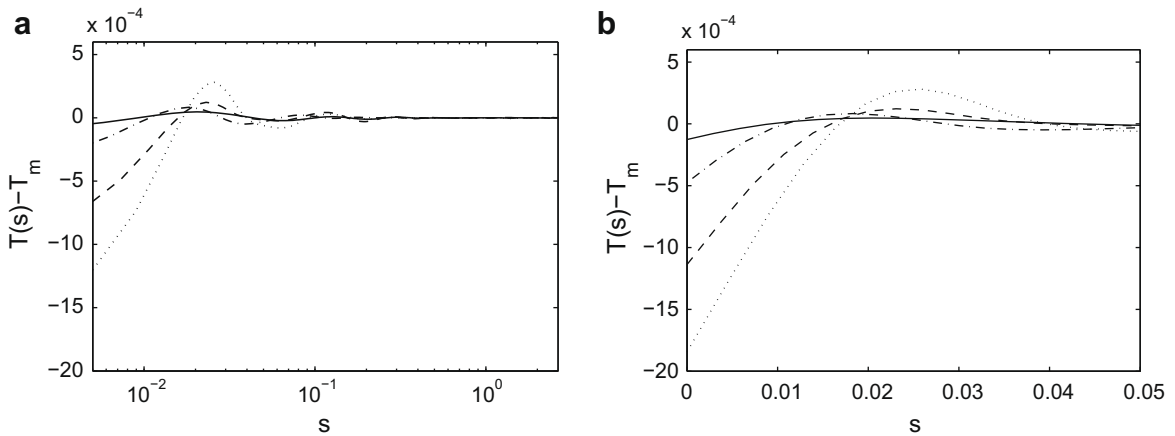


Fig. 8. Deviations of the interface temperature $T|_{\Gamma_{SL}}$ from T_m along the interface Γ_{SL} for different imposed contact angles: (solid) $\alpha_m = 60^\circ$, (dash-dotted) $\alpha_m = 50^\circ$ (dashed) $\alpha_m = 40^\circ$, and (dotted) $\alpha_m = 30^\circ$; figure (a) represents the entire interface Γ_{SL} and uses the logarithmic scale with the origin cut out for the independent variable s , whereas figure (b) shows the magnification of the neighborhood of the contact point B using the linear scale.

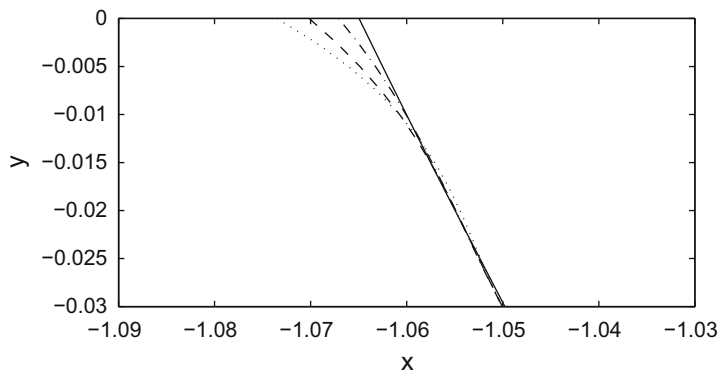


Fig. 9. Positions of the interface Γ_{SL} corresponding to different values of the contact angle α_m prescribed at B : (solid) no contact angle prescribed (case A), (dash-dotted) $\alpha_m = 50^\circ$, (dashed) $\alpha_m = 40^\circ$, and (dotted) $\alpha_m = 30^\circ$.

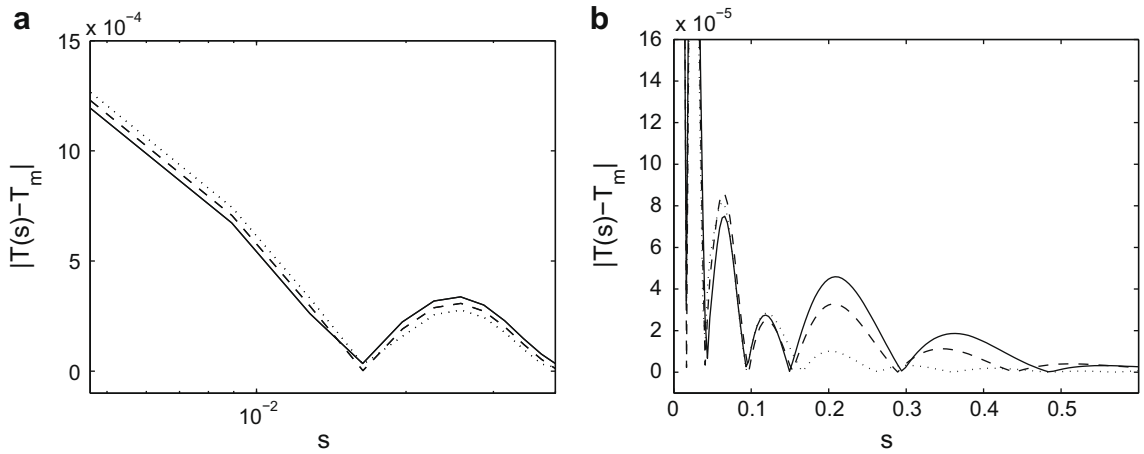


Fig. 10. Deviations of the interface temperature $T|_{\Gamma_{SL}}$ from T_m along the interface Γ_{SL} for different values of the parameter ℓ : (solid) $\ell = 5 \times 10^{-4}$, (dashed) $\ell = 10^{-3}$, and (dotted) $\ell = 10^{-1}$; figure (a) shows the neighborhood of the contact point and uses the logarithmic scale with the origin cut out for the independent variable s , whereas figure (b) shows a larger part of the interface Γ_{SL} using the linear scale.

$$Q_1(\ell) \triangleq 2 \int_{\Gamma_{SL}} \frac{|T - T_m|}{\max |T - T_m|} ds, \tag{47a}$$

$$Q_2(\ell) \triangleq \frac{\int_{\Gamma_{SL}} s(T - T_m)^2 ds}{\int_{\Gamma_{SL}} (T - T_m)^2 ds}. \tag{47b}$$

We note that when $\ell \rightarrow \infty$, the distance measures Q_1 and Q_2 do not vanish, but instead approach some finite limiting values $\tilde{Q}_i \triangleq \lim_{\ell \rightarrow \infty} Q_i(\ell)$, $i = 1, 2$. Therefore, in Fig. 11 we plot the normalized quantities $\left(\frac{Q_i(\ell)}{\tilde{Q}_i} - 1\right)$, $i = 1, 2$, as a function of the parameter ℓ . The results reported in Fig. 11 were obtained with the resolution $h = 5 \times 10^{-6}$. We note that the data reveals a linear scaling for both plotted quantities which, given the log–log scale used in the plot, implies the following approximate behavior for the quantities Q_1 and Q_2

$$\left(\frac{Q_i(\ell)}{\tilde{Q}_i} - 1\right) \approx a\ell^{-1} \Rightarrow Q_i(\ell) \approx \tilde{Q}_i + b\ell^{-1}, \quad i = 1, 2, \tag{48}$$

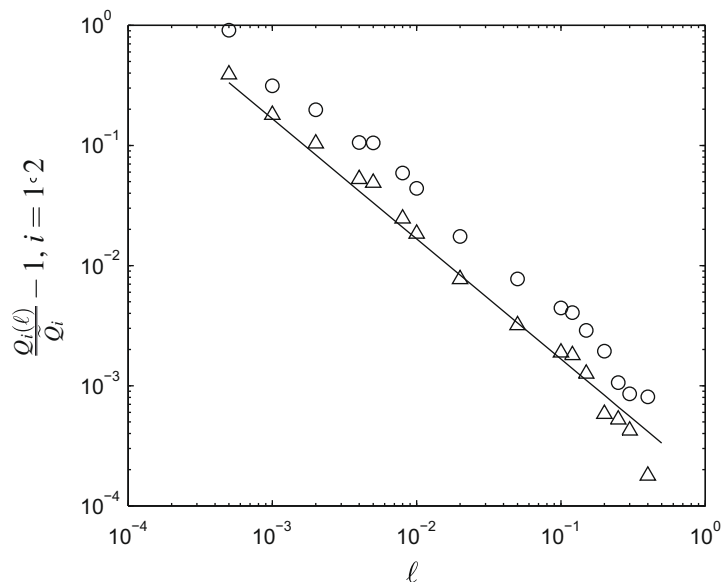


Fig. 11. Scaling of (triangles) $\left(\frac{Q_1(\ell)}{\tilde{Q}_1} - 1\right)$ and (circles) $\left(\frac{Q_2(\ell)}{\tilde{Q}_2} - 1\right)$ as a function of the parameter ℓ . The solid line has the slope ℓ^{-1} .

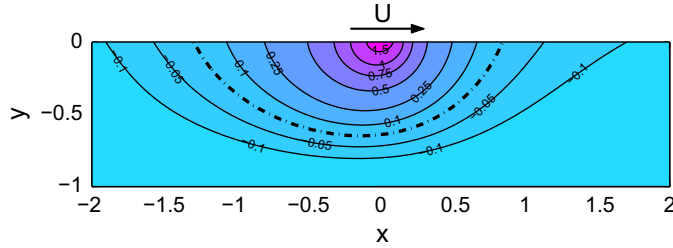


Fig. 12. Temperature isolines $\tilde{T}(x,y) - T_m$ and (dashed line) the interface Γ_{SL} in the solution of the problem in case C.

where a and b are some positive constants. Empirical relation (48) implies that our measures Q_1 and Q_2 of the distance from the contact point where relation (9a) significantly deviates from (7) depends on the parameter ℓ and this dependence has a well-defined universal behavior. More specifically, this distance has a minimum value given by $\tilde{Q}_i, i = 1, 2$, and grows proportionally to ℓ^{-1} . Thus, the parameter ℓ in (11) can be interpreted as the inverse of the length-scale over which the contact points affect the temperature distribution along the interface in our closure model. Remarkably, as is evident from Fig. 11, the scaling expressed by Eq. (48) holds over about three orders of magnitude in ℓ . As regards the bound from below on this interval, it corresponds to $Q_i(\ell)$ on the order of the length of the entire interface, i.e., (9a) deviates from (7) everywhere on Γ_{SL} (cf. Fig. 5a). On the other hand, the upper bound on this scaling range is related to the numerical resolution which determines the accuracy with which the integrals in (47b) are evaluated.

We finally come to case C corresponding to the heat source moving at a constant velocity $U\mathbf{e}_x$, which provides a simplified model of weld pool formation in a welding process. In general, such process is unsteady and is described by the time-dependent versions of equations (1b). However, assuming that the time-scale associated with the free boundary formation is much shorter than the time-scale of the heat source translation, this phenomenon may be regarded as quasi-stationary in a moving frame of reference given by the transformation $\tilde{\mathbf{x}}(t, \mathbf{x}) \triangleq \mathbf{x} - tU\mathbf{e}_x$. Therefore, defining $\tilde{T}(t, \tilde{\mathbf{x}}(t, \mathbf{x})) \triangleq T(t, \mathbf{x})$ we obtain

$$\frac{\partial T}{\partial t} \Big|_{\mathbf{x}} = \frac{\partial \tilde{T}}{\partial t} \Big|_{\tilde{\mathbf{x}}} - U \frac{\partial \tilde{T}}{\partial \tilde{x}} \Big|_t, \tag{49}$$

so that the assumed stationarity in the moving frame of reference $\frac{\partial \tilde{T}}{\partial t} \Big|_{\tilde{\mathbf{x}}} \equiv 0$ yields the following “corrected” forms of equations (1)

$$-\tilde{\nabla} \cdot (k_S \tilde{\nabla} \tilde{T}) = U \frac{\partial \tilde{T}}{\partial \tilde{x}} \quad \text{in } \Omega_S, \tag{50a}$$

$$-\tilde{\nabla} \cdot (k_L \tilde{\nabla} \tilde{T}) = U \frac{\partial \tilde{T}}{\partial \tilde{x}} \quad \text{in } \Omega_L, \tag{50b}$$

where $\tilde{\nabla}$ represents differentiation with respect to the transformed variable $\tilde{\mathbf{x}}$. Eq. (50b) are supplemented with boundary conditions (2)–(4) as used in the original system together with the time-dependent version of condition (5), namely

$$-\left[k \frac{\partial \tilde{T}}{\partial \mathbf{n}} \right]_S^L = LU(\mathbf{e}_x \cdot \mathbf{n}) \quad \text{on } \Gamma_{SL}.$$

Following the procedure described in Section 3, we obtain the corresponding adjoint system

$$-\tilde{\nabla} \cdot (k_S \tilde{\nabla} \tilde{T}^*) = -U \frac{\partial \tilde{T}^*}{\partial \tilde{x}} \quad \text{in } \Omega_S, \tag{51a}$$

$$-\tilde{\nabla} \cdot (k_L \tilde{\nabla} \tilde{T}^*) = -U \frac{\partial \tilde{T}^*}{\partial \tilde{x}} \quad \text{in } \Omega_L. \tag{51b}$$

The boundary conditions and expressions characterizing the gradient remain the same as in (31)–(34) and (38), respectively. Fig. 12 illustrates the temperature distribution and the position of the interface obtained in this case, where we used $U = 100$ and did not impose the contact angles. We note a deformation of the shape of the interface Γ_{SL} induced by the advection. An analogous approach was applied in [33] to optimize complex 3D thermo-fluid phenomena occurring in welding processes and involving the conservation of mass, momentum and energy in the presence of free boundaries and capillary effects.

6. Conclusions

This paper is concerned with the formulation of the Stefan problem involving contact points (lines) as a PDE optimization problem where the shape of the interface serves as the control variable. By allowing for a systematic deviation of the interface temperature $T|_{\Gamma_{SL}}$ from the constant melting temperature T_m it is possible to accommodate a prescribed macroscopic

contact angle α_m which is known to be a constitutive property of the material [19]. Since the RHS of expression (9a) is generally given in terms of unknown microscopic quantities, the proposed method can be regarded as a closure model for the governing system of equations. In this sense it is related to “subgrid-scale” models used commonly in computations of high Reynolds number turbulent flows [34]. The key difference is that while in subgrid-scale models for turbulence simulations the unresolved (modeled) quantities are defined at length-scales smaller than the grid size everywhere in the solution domain, in the present problem the closure model mostly impacts the neighborhood of the contact point, and the characteristic dimension of this neighborhood is controlled by the parameter ℓ . Our proposed approach to dealing with the contact point singularities in the Stefan problem has similarities to the treatment of contact points in the momentum (Navier–Stokes) equation which results in the Navier boundary conditions [35,36]. In analogy to the relaxation of Dirichlet boundary condition (7) for the temperature, in the Navier boundary condition the no-slip constraint on the velocity is replaced with a formulation allowing for a finite slip velocity in a neighborhood of the contact point. As is the case in our problem too, the dimension of this neighborhood (i.e., the “slip length”) is a macroscopic parameter.

The Stefan problem formulated in this way turns out to be a shape optimization problem, and the shape differential calculus is a key enabler of a computational algorithm employed to solve such a problem. We use a suitably-defined adjoint system to determine the shape gradient of the cost functional, and the main novelty here is a definition of the gradient consistent with the presence of the contact points. Optimization was performed using smoothed (Sobolev) shape gradients, which was shown in [29] to have the effect of regularization. Our computational examples confirm the efficiency of the proposed approach on a few test cases. The results obtained reveal a systematic deviation of the interface temperature from T_m in the neighborhood of a contact point as a function of the imposed contact angle α_m . The length-scale over which this deviation occurs exhibits a universal behavior with respect to the parameter ℓ . The results reported in Section 5 show that for vanishing values of ℓ this length-scale becomes comparable with the characteristic dimension of the interface, while the magnitude of the deviation vanishes. On the other hand, for increasing values of ℓ , this length-scale decreases and approaches a (small) fixed distance while the magnitude of the deviation increases.

As regards the computational performance, we remark that despite the formal linearity of Eq. (1), the Stefan problem is in fact *geometrically* nonlinear, hence its computational solution must necessarily involve some form of iterations, regardless of the method used. It should be stressed that since the interface Γ_{SL} is the control variable, it is always represented explicitly and as such does not have to be reconstructed a posteriori to satisfy the interface conditions. Another novelty of the proposed approach is that in this way we relax temperature condition (7), rather than flux condition (5) as was proposed in some earlier studies, which is shown to be thermodynamically more consistent. We also emphasize that the presented method admits a straightforward generalization to three dimensions. Our future work on this class of problems will involve extensions of the present method to a time-dependent problem and problems involving transport of the momentum modeled by the Navier–Stokes equation [33]. We also intend to apply this method to the study of actual inverse problems where some input parameters need to be optimized to meet certain objectives. On the technical side, an interesting question is to determine Sobolev gradients for general perturbations \mathbf{Z} (i.e., not restricted to the form $\mathbf{Z} = \zeta \mathbf{e}_r$).

Acknowledgments

The authors wish to thank Donn Glander, Arian Novruzi and Nikolas Provatas for many helpful discussions. The funding for this research was provided by the Natural Sciences and Engineering Research Council of Canada (the Collaborative Research and Development Program), the General Motors of Canada, Ltd., and the Ontario Centres of Excellence – Centre for Materials and Manufacturing, and is gratefully acknowledged.

Appendix A. Regularity of solutions of the classical Stefan problem in domains with corners

In this appendix we present the proof of existence of a smooth solution belonging to the Hölder class $C^{1,\alpha}$ of the free-boundary problem defined in (1)–(5) and (7), provided a certain regularity of the boundary $\Gamma_{SG} \cup \Gamma_{LG}$ and corresponding boundary data can be guaranteed. We emphasize that this proof refers to the situation where *no* contact angles are imposed. The idea of the proof is to reduce our problem to a form which can be treated using results from the existing literature on elliptic boundary value problems in domains with corners (e.g., [37]). We will first consider the case of $k_S = k_L \triangleq k$, and then extend this result to the case of $k_S \neq k_L$. We begin by stating the following assumptions:

- the boundary $\Gamma_{SG} \cup \Gamma_{LG}$ is C^2 ,
- the Dirichlet and Neumann data (cf. (2b) and (3))

$$\begin{cases} T_s & \text{on } \Gamma_S, \\ \varphi_{SG} & \text{on } \Gamma_{SG}, \\ \varphi_{LG} & \text{on } \Gamma_{LG} \end{cases} \quad (\text{A.1})$$

is in the space $W^{3/2,p}(\Gamma_S) \times W^{1/2,p}(\Gamma_{SG} \cup \Gamma_{LG})$, $p \geq 2$,

- compatibility condition (4) is satisfied,
- $\forall \mathbf{x} \in \Gamma_S, T_s < T_m$ and $\exists \mathbf{x} \in \Gamma_{LG}, T|_{\mathbf{x}} > T_m$.

We note that the last assumption guarantees the existence of contact points on the top surface. In regard to the case $k_S = k_L$, the trace theorems in [21] (Section 1.5) allow us to conclude that there exists a unique $\bar{T} \in W^{2,p}(\mathbb{R}^2)$, such that its trace $\{\gamma|_{\Gamma_S}(\bar{T}), \gamma|_{\Gamma_{SG} \cup \Gamma_{LG}}(\partial\bar{T}/\partial n)\}$ is in $W^{3/2,p}(\Gamma_S) \times W^{1/2,p}(\Gamma_{SG} \cup \Gamma_{LG})$. Moreover, for $p > 2$ one has the following Sobolev imbedding theorem [18]

$$W^{2,p}(\bar{\Omega}_{SL}) \subseteq C^{1,\alpha}(\bar{\Omega}_{SL}), \quad 0 < \alpha \triangleq 1 - 2/p < 1. \tag{A.2}$$

The Stefan problem defined in (1)–(5) and (7) and with $k_S = k_L$ may thus be reduced to a boundary value problem with the homogeneous boundary conditions for the unknown $(T - \bar{T}) \in H^1(\Omega_{SL})$ satisfying

$$\int_{\Omega_{SL}} \bar{k} \nabla(T - \bar{T}) \cdot \nabla v \, d\Omega = \int_{\Omega_{SL}} \nabla \cdot (\bar{k} \nabla \bar{T}) v \, d\Omega \quad \forall v \in H^1(\Omega_{SL}). \tag{A.3}$$

The following result is a special case of the theorem proved in [37] and is important for the study of the regularity of the solution of (A.3)

Theorem A.1. *We assume that $p \geq s + 2, s \in \{-1, 0, 1, \dots\}$. Let $T - \bar{T}$ be a solution of problem (A.3) with $\nabla \cdot (\bar{k} \nabla \bar{T}) \in W^{s,p}(\Omega_{SL})$. Then $T - \bar{T} \in W^{2+s,p}(\Omega_{SL})$ if and only if $\forall \lambda \notin \{2l + 1 | l \in \mathbb{Z}, l \neq 0\}, 0 \leq \text{Re}(\lambda) \leq s + 2 - 2/p$.*

We note that $\{2l + 1 | l \in \mathbb{Z}, l \neq 0\}$ is the set of the eigenvalues of some Laplace–Beltrami operator corresponding to our particular boundary value problem. This set is determined by the type of the boundary conditions imposed on the boundary segments of $\partial\Omega_{SL}$ and by the measures of the angles between these segments [37]. When $p > 2$, then $1 < 2 - 2/p \leq 2$, and the assumptions of Theorem A.1 are satisfied for $s = 0$ implying that the solution T and its gradient are continuous up to the boundary. If now the solution T assumes the value T_m somewhere inside Ω_{SL} , there must exist an entire isoline satisfying the classical Stefan condition (7).

Let us now turn to the less trivial case when $k_S > k_L$. We introduce a new variable $\hat{T} \in H^1(\Omega_{SL})$ which satisfies a system equivalent to (1)–(5) and (7), namely

$$-\Delta \hat{T} = 0 \quad \text{in } \Omega_S \cup \Omega_L, \tag{A.4a}$$

$$-\frac{\partial \hat{T}}{\partial n} = \frac{2\varphi_{SG}}{k_S + k_L} \quad \text{on } \Gamma_{SG}, \tag{A.4b}$$

$$-\frac{\partial \hat{T}}{\partial n} = \frac{2\varphi_{LG}}{k_S + k_L} \quad \text{on } \Gamma_{LG}, \tag{A.4c}$$

$$\hat{T} = (1 + \rho)T_s \quad \text{on } \Gamma_S, \tag{A.4d}$$

$$\left[\frac{\partial \hat{T}}{\partial n} \right]_S^L = 0 \quad \text{on } \Gamma_{SL}, \tag{A.4e}$$

where $\rho \triangleq (k_S - k_L)/(k_S + k_L)$. According to the result proved above, there exists a solution of (A.4e) in the space $C^{1,\alpha}(\bar{\Omega}_{SL})$. Moreover, one can identify an isoline corresponding to each value assumed by this solution inside the domain Ω_{SL} . Supposing that this value is now $(1 + \rho)T_m$, one can verify that

$$T = \begin{cases} \frac{\hat{T} - 2\rho T_m}{1 - \rho} & \text{in } \Omega_L, \\ \frac{\hat{T}}{1 + \rho} & \text{in } \Omega_S, \end{cases} \tag{A.5}$$

and Γ_{SL} defined as the isoline corresponding to \hat{T} provides an unique $C^{1,\alpha}(\bar{\Omega}_L) \times C^{1,\alpha}(\bar{\Omega}_S)$ solution of original system (1)–(5) also satisfying classical Stefan condition (7). This guarantees the existence of contact points on the top surface.

References

[1] B. Amar, Y. Pomeau, Growth of faceted needle crystals: theory, Europhys. Lett. 6 (1988) 609–614.
 [2] M.E. Gurtin, J. Matias, Thermomechanics and the formulation of the Stefan problem for fully faceted interfaces, Quart. Appl. Math. 53 (1995) 761–782.
 [3] S. Schiaffino, A.A. Sonin, Motion and arrest of a molten contact line on a cold surface: an experimental study, Phys. Fluids 9 (1997) 2217–2226.
 [4] S. Schiaffino, A.A. Sonin, On the theory for the arrest of an advancing molten contact line on a cold solid of the same material, Phys. Fluids 9 (1997) 2227–2233.
 [5] P. Neittaanmaki, J. Sprekels, D. Tiba, Optimization of Elliptic Systems: Theory and Applications, Springer, 2006.
 [6] H.W. Alt, L.A. Caffarelli, Existence and regularity for a minimum problem with free boundary, J. Reine Angew. Math. 325 (1981) 105–144.
 [7] J.-P. Zolésio, Weak shape formulation of free boundary problems, Ann. Scuola Norm. Sup. Pisa Cl. Sci. 21 (I) (1994) 11–44.
 [8] K.-H. Hoffmann, D. Tiba, Fixed domain methods in variable domain problems, in: J.I. Diaz, (Ed.), Free Boundary Problems: Theory and Applications Pitman Res. Notes Math. Ser., vol. 323, Longman Sci. Tech, Harlow, 1995, p. 123–146.
 [9] S.P. Okhezin, Optimal shape design for parabolic system and two-phase Stefan problem, in: Free Boundary Problems in Continuum Mechanics, Birkhauser, 1992, pp. 239–244.
 [10] J. Sokolowski, J.-P. Zolésio, Introduction to Shape Optimization. Shape Sensitivity Analysis, Springer, 1992.
 [11] T. Männikkö, P. Neittaanmäki, D. Tiba, A rapid method for the identification of the free boundary in two-phase Stefan problems, IMA J. Numer. Anal. (1994) 411–420.
 [12] T. Tiihonen, Shape optimization and trial methods for free boundary problems, RAIRO Modél. Math. Anal. Numér. 31 (1997) 805–825.

- [13] K. Kärkkäinen, T. Tiihonen, Free surfaces: shape sensitivity analysis and numerical methods, *Int. J. Numer. Methods Eng.* 44 (1999) 1079–1098.
- [14] J. Haslinger, T. Kozubek, K. Kunisch, G. Peichl, Shape optimization and fictitious domain approach for solving free boundary problems of Bernoulli type, *Comput. Optim. Appl.* 26 (2003) 231–251.
- [15] R.D. Donaldson, B.R. Wetton, Solving steady interface problems using residual velocities, *IMA J. Appl. Math.* 71 (2006) 877–897.
- [16] K. Eppler, H. Harbrecht, Efficient treatment of stationary free boundary problems, *Appl. Numer. Math.* 56 (2006) 1326–1339.
- [17] K. Eppler, H. Harbrecht, R. Schneider, On convergence of elliptic shape optimization, *SIAM J. Control Optim.* 46 (2007) 61–83.
- [18] R.A. Adams, J.F. Fournier, *Sobolev Spaces*, Elsevier, 2005.
- [19] M.E. Gurtin, *Thermomechanics of Evolving Phase Boundaries in the Plane*, Oxford University Press, 1993.
- [20] S.H. Davis, *Theory of Solidification*, Cambridge University Press, 2001.
- [21] P. Grisvard, *Elliptic Problems in Nonsmooth Domains*, Pitman Published, 1985.
- [22] M. Dauge, *Elliptic Boundary Value Problems in Corner Domains – Smoothness and Asymptotics of Solutions*, Lecture Notes in Mathematics, vol. 1341, Springer-Verlag, Berlin, 1988.
- [23] D.M. Anderson, S.H. Davis, Local fluid and heat flow near contact lines, *J. Fluid Mech.* 268 (1994) 231–265.
- [24] P. Rybka, A crystalline motion: uniqueness and geometric properties, *SIAM J. Appl. Math.* 57 (1997) 53–72.
- [25] J. Simon, Differentiation with respect to domain in boundary value problems, *Numer. Funct. Anal. Optimiz.* 2 (7&8) (1980) 649–687.
- [26] M.S. Berger, *Nonlinearity and Functional Analysis*, Academic Press, 1977.
- [27] J. Nocedal, S. Wright, *Numerical Optimization*, Springer, 2002.
- [28] M.D. Gunzburger, *Perspectives in Flow Control and Optimization*, SIAM, Philadelphia, 2003.
- [29] B. Protas, T. Bewley, G. Hagen, A comprehensive framework for the regularization of adjoint analysis in multiscale PDE systems, *J. Comput. Phys.* 195 (1) (2004) 49–89.
- [30] J. Neuberger, *Sobolev Gradients and Differential Equations*, Springer, 1997.
- [31] See <www.comsol.com>.
- [32] C. Homescu, I.M. Navon, Z. Li, Suppression of vortex shedding for flow around a circular cylinder using optimal control, *Int. J. Numer. Meth. Fluids* 38 (2002) 43–69.
- [33] O. Volkov, B. Protas, W. Liao, D. Glander, Adjoint-based optimization of thermo-fluid phenomena in welding processes, *J. Eng. Math.* in press, (accepted for publication, doi:10.1007/s10665-009-9292-0).
- [34] S.B. Pope, *Turbulent Flows*, Cambridge University Press, 2000.
- [35] Y.D. Shikhmurzaev, *Capillary Flows with Forming Interfaces*, Taylor & Francis, 2007.
- [36] T. Qian, X.-P. Wang, P. Sheng, A variational approach to moving contact line hydrodynamics, *J. Fluid Mech.* 564 (2006) 333–360.
- [37] M. Dauge, Neumann and mixed problems on curvilinear polyhedra, *Int. Eq. Oper. Th.* 15 (1992) 227–261.